
PQMass: Probabilistic Assessment of the Quality of Generative Models using Probability Mass Estimation

Pablo Lemos^{1 2 3 4 5} Sammy Sharief^{1 2 3} Nikolay Malkin^{1 3} Laurence Perreault-Levasseur^{* 1 2 3 4 6 7}
Yashar Hezaveh^{* 1 2 3 4 6 7}

Abstract

We propose a comprehensive sample-based method for assessing the quality of generative models. The proposed approach enables the estimation of the probability that two sets of samples are drawn from the same distribution, providing a statistically rigorous method for assessing the performance of a single generative model or the comparison of multiple competing models trained on the same dataset. This comparison can be conducted by dividing the space into non-overlapping regions and comparing the number of data samples in each region. The method only requires samples from the generative model and the test data. It is capable of functioning directly on high-dimensional data, obviating the need for dimensionality reduction. Significantly, the proposed method does not depend on assumptions regarding the density of the true distribution, and it does not rely on training or fitting any auxiliary models. Instead, it focuses on approximating the integral of the density (probability mass) across various sub-regions within the data space.

1. Introduction

Generative modeling has become an important and ubiquitous topic in machine learning. The goal of generative modeling is to approximate a distribution given a set of samples from the distribution. Generative machine learning has witnessed the development of a succession of methods for distribution approximation, including variational autoencoders (VAEs, Kingma & Welling, 2013), generative adversarial networks (GANs, Goodfellow et al., 2014), normalizing flows (Rezende & Mohamed, 2015), and score-based (diffusion) generative models (Ho et al., 2020b).

^{*}Equal contribution ¹Mila – Québec Artificial Intelligence Institute ²Ciela Institute ³Université de Montréal ⁴CCA – Flatiron Institute ⁵Dreamfold ⁶Perimeter Institute ⁷Trottier Space Institute. Correspondence to: Pablo Lemos <pablo.lemos@umontreal.ca>.

With advancements in generative models, evaluating their performance using rigorous, clearly defined metrics and criteria has become increasingly essential. Disambiguating true from modeled distributions is especially pertinent in light of the growing emphasis on AI safety within the community, as well as in scientific domains where stringent standards of rigor and uncertainty quantification are needed for the adoption of machine learning methods. When evaluating generative models, we are interested in three qualitative properties (Stein et al., 2023; Jiralerspong et al., 2023): **Fidelity** refers to the quality and realism of individual outputs generated by a model. It assesses how indistinguishable each generated sample is from real data. **Diversity** pertains to the range and variety of outputs a model can produce. For example, a model that misses a mode in the training data, producing no samples of the given mode, has lower diversity. **Novelty** refers to the ability of a model to generate new, previously unseen samples that are not replicas of the training data yet are coherent and meaningful within the context of the task. Essentially, it means appropriately interpolating the regions in between the training data in higher-density regions.

There have been two classes of methods for evaluating generative models: **sample-based methods**, which compare generated samples to true samples directly, and **likelihood-based methods**, which make use of the likelihood of the data under the model. It has been observed that likelihood-based methods, such as data negative log-likelihood (NLL), show too much variance to be useful in practice and are ‘saturated’ on standard benchmarks, *i.e.*, they do not correlate well with sample fidelity, particularly in high-dimensional settings (Theis et al., 2015; Nalisnick et al., 2018; Nowozin et al.; Yazici et al., 2020; Le Lan & Dinh, 2021). On the other hand, most sample-based methods cannot measure the combination of fidelity, diversity, and novelty. For example, the Fréchet Inception Distance (FID; Heusel et al., 2017) and the Inception Score (IS; Salimans et al., 2016; Sajjadi et al., 2018) measure fidelity and diversity, but not novelty, while precision and recall (Salimans et al., 2018) measure only fidelity and diversity, respectively; and authenticity (Alaa et al., 2022) measures only novelty. Recently, the Feature Likelihood Score (FLS; Jiralerspong et al., 2023)

was proposed as a measure that captures fidelity, novelty, and diversity. However, FLS essentially relies on the approximation of the underlying distribution by a Gaussian mixture model and consequently requires feature extraction and compression for high-dimensional models using an auxiliary model.

In this work, we propose **PQMass**, a general statistical framework for evaluating the quality of generative models that measures the combination of fidelity, diversity, and novelty and scales well to high dimensions without the need for dimensionality reduction. PQMass allows us to accurately estimate the relative probability of a generative model given a test dataset by examining the *probability mass* of the data over appropriately chosen regions.

The main idea motivating PQMass is that given a sub-region of the entire space, the number of data points lying in the region follows a binomial distribution with a parameter equal to the region’s true probability mass (which is unknown and should be marginalized). By extension, given a partition of the space into regions, the counts of points falling into the regions follow a multinomial distribution. PQMass uses two-sample tests on these multinomial distributions’ parameters for prudently selected regions defined by Voronoi cells. This approach gives us a p-value, measuring the quality of a generative model (the probability of a model given the training data). It also allows the comparison of various competing models by analyzing the ratio of their probabilities.

Since PQMass works with the *integrals* of the true and estimated probability density functions over regions, it does not make any assumptions about the true underlying density field. PQMass is also computationally efficient and scales well with the dimensionality of the data, allowing us to directly evaluate generative models of high-dimensional data, such as images, without the need for feature extraction or compression. Finally, PQMass is general and flexible, allowing the evaluation of generative models on any type of data, including images and time series.

Our contributions are the following: In §2, we introduce the theoretical framework for PQMass. In §3, we introduce an algorithmic instantiation of the framework. In §4, we present experiments on synthetic and real-world datasets and compare PQMass with prior methods.

2. Theoretical Framework

Our problem statement is the following. We have two sets of samples $\{x_i\}_{i=1\dots n} \sim p(x)$ and $\{y_i\}_{i=1\dots m} \sim q(y)$, where both p and q have support in some region $X \subseteq \mathbb{R}^d$. We are interested in testing the statistical hypothesis that $p = q$, that is, the two samples came from the same distribution.

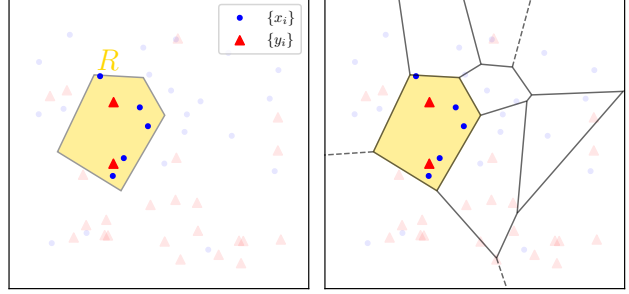


Figure 1. An illustration of the statistic computed by PQMass. *Left:* We start with two sets of samples $\{x_i\}_{i=1\dots n} \sim p(x)$ and $\{y_i\}_{i=1\dots m} \sim q(y)$, shown as red and blue points, respectively. For a given region $R \subseteq X$, the fraction of samples in R for each set of samples follows a binomial distribution, with parameters n and $\mathbb{P}_p(R)$ for the red samples, and m and $\mathbb{P}_q(R)$ for the blue samples. We can use this binomial distribution to estimate the probability that both binomial distributions are the same. *Right:* If we can build non-overlapping regions $\{R_i\}_{i=1\dots n_R}$, for example, using a Voronoi tessellation, the distribution of samples in the regions follows a multinomial distribution, for each set of samples. PQMass performs hypothesis tests on equality of the two multinomial distributions to obtain a p-value.

2.1. Measuring Equivalence

We recall an elementary fact from the foundations of probability: two probability distributions $p(x)$ and $q(x)$ over a measurable region $X \subseteq \mathbb{R}^d$ are equivalent if they are equal as measures, *i.e.*,

$$\mathbb{P}_p(R) = \mathbb{P}_q(R) \quad \forall R \subseteq X, R \text{ measurable.} \quad (1)$$

Following this fact, we can measure whether two distributions are equivalent by estimating, using samples drawn from these distributions, whether the mass they assign to a large number of finite, arbitrary regions is equal.

We will now introduce a method for estimating this probability. We start with the following simple observation:

Lemma 2.1. *Given a set of samples $\{x_i\}_{i=1\dots n} \sim p(x)$, the probability in a region $R \subseteq X$ can be approximated by the proportion of samples in R :*

$$\mathbb{P}_p(R) = \mathbb{E}_{x \sim p(x)} [\mathbb{1}(x \in R)] \approx \frac{1}{n} |\{i : x_i \in R\}|. \quad (2)$$

This estimate is unbiased, and in the limit of infinite samples, this approximation becomes exact (i.e., the estimator is consistent).

Proof. We start by defining the random variable X as

$$X = \begin{cases} 1 & \text{if } x \in R \\ 0 & \text{otherwise} \end{cases} \quad (3)$$

We have that

$$\mathbb{E}_{x \sim p(x)} [X] = \mathbb{P}_p(R) \quad (4)$$

We can approximate this expectation by the empirical mean

of the samples:

$$\mathbb{E}_{x \sim p(x)} [X] \approx \frac{1}{n} \sum_{i=1}^n X_i = \frac{1}{n} \sum_{i=1}^n \mathbb{1}(x_i \in R) \quad (5)$$

which is the proportion of samples in R . \square

In the following, we will use the notation

$$k(\mathbf{x}, R) \equiv \sum_{i=1}^n \mathbb{1}(x_i \in R). \quad (6)$$

Here, $k(\mathbf{x}, R)$ is the number of samples of the entire dataset, \mathbf{x} , in a region R . We can approximate the probability mass in a region R by the proportion of samples in \mathbf{x} that lie in R . We can now use this approximation to measure whether two sets of samples are equivalent, by measuring whether the proportion of samples in a large number of finite regions is the same for both sets of samples.

A simple, non-probabilistic method for assessing the equivalence of two datasets might involve directly comparing their respective proportions. Nonetheless, this paper will demonstrate a framework for conducting a more comprehensive analysis. This approach aims to quantify the probability that the two datasets are equivalent, thereby providing a rigorous statistical measure of their similarity.

2.2. Quantifying the Probability in a Region: A Frequentist Approach

We will now introduce a method for measuring this proportion. First, we notice the following important property:

Lemma 2.2. *Given a set of samples $\{x_i\}_{i=1 \dots n} \sim p(x)$, the number of samples in a region $R \subseteq X$ follows a binomial distribution:*

$$k(\mathbf{x}, R) \sim \mathcal{B}(n, \mathbb{P}_p(R)) \quad (7)$$

This means that, given two sets of samples $\{x_i\}_{i=1 \dots n} \sim p(x)$ and $\{y_i\}_{i=1 \dots m} \sim q(y)$, we can estimate the value of $\mathbb{P}_p(R)$ and $\mathbb{P}_q(R)$, using $\hat{p}_R \equiv k(\mathbf{x}, R)/n$ and $\hat{q}_R \equiv k(\mathbf{y}, R)/m$ as estimators respectively.

We can easily extend this result to any number of non-overlapping regions $\{R_i\}_{i=1 \dots n_R}$, by noticing that the number of samples in each region follows a multinomial distribution:

$$\{k(\mathbf{x}, R_i)\}_{i=1 \dots n_R} \sim \mathcal{M}\left(n, \{\mathbb{P}_p(R_i)\}_{i=1 \dots n_R}\right). \quad (8)$$

Therefore, given a set of regions $\{R_i\}_{i=1 \dots n_R}$, we can estimate the probability that both sets of samples are equivalent by measuring whether the multinomial distributions are the same. We first discuss how to approach this problem from a frequentist perspective. We will discuss the Bayesian approach in the next subsection.

In the frequentist approach, there are multiple ways to measure whether two multinomial distributions are the

same (see, e.g., Anderson et al., 1974; Zelterman, 1987; Plunkett & Park, 2019; Bastian et al., 2024). In this paper, we use one of the simplest methods, the Pearson χ^2 test (Rao, 1948). We will explore alternative methods in future work. For reviews on this test, see (Rao, 2002). We start by defining the expected counts for each region:

$$\hat{N}_{x,i} \equiv n\hat{p}_{R_i}, \quad \hat{N}_{y,i} \equiv m\hat{p}_{R_i}, \quad (9)$$

where:

$$\hat{p}_{R_i} \equiv \frac{k(\mathbf{x}, R_i) + k(\mathbf{y}, R_i)}{n + m}. \quad (10)$$

We can then define the χ_{PQM}^2 statistic using the definition of the Pearson chi-squared:

$$\chi_{\text{PQM}}^2 \equiv \sum_{i=1}^{n_R} \left[\frac{(k(\mathbf{x}, R_i) - \hat{N}_{x,i})^2}{\hat{N}_{x,i}} + \frac{(k(\mathbf{y}, R_i) - \hat{N}_{y,i})^2}{\hat{N}_{y,i}} \right]. \quad (11)$$

This statistic follows a χ^2 distribution with $n_R - 1$ degrees of freedom. Therefore, we can calculate the p-value of the test as

$$\text{p-value}(\chi_{\text{PQM}}^2) \equiv \int_{-\infty}^{\chi_{\text{PQM}}^2} \chi_{n_R-1}^2(z) dz. \quad (12)$$

This p-value provides an estimate of the probability that the two sets of samples are equivalent.

With that, we can summarize this section into the main theoretical result of this paper:

Given any sampling distribution, or generative model, if two sets of samples are generated from the same distribution, then the statistic χ_{PQM}^2 follows a chi-square distribution with $n_R - 1$ degrees of freedom.

We can then use this result to quantify how different the two sets of samples are.

2.3. Quantifying the Probability in a Region: A Bayesian Approach

We can also use a Bayesian approach to quantify the probability in a set of regions. Once again, we know that the proportion of samples in a set of regions $\{R_i\}_{i=1 \dots n_R}$ follows a multinomial distribution. Therefore, we can use the closed-form likelihood of the multinomial distribution to calculate the probability of the proportion of samples in a region R given a set of samples $\{x_i\}_{i=1 \dots n} \sim p(x)$:

$$\mathcal{L}_x \equiv \mathbb{P}(\{x_i\}_{i=1 \dots n} | \mathbb{P}_p, \{R_i\}_{i=1 \dots n_R}) = \binom{n}{k(\mathbf{x}, R_1), \dots, k(\mathbf{x}, R_{n_R})} \prod_i \mathbb{P}_p(R_i)^{k(\mathbf{x}, R_i)}, \quad (13)$$

and similarly for \mathcal{L}_y . In a Bayesian approach, we can use the posterior predictive distribution (PPD) to calculate the probability of finding the number of samples, $k(\mathbf{y}, R)$, in a region R given the number of samples from the other set,

$k(\mathbf{x}, R)$, in the same region:

$$\begin{aligned} & \mathbb{P}(\{y_i\}_{i=1\dots m} \mid \{x_i\}_{i=1\dots n}, \{R_i\}_{i=1\dots n_R}) = \\ & \int d\lambda_1 d\lambda_2 \dots d\lambda_{n_R} \mathbb{P}(\{y_i\}_{i=1\dots m} \mid \{\lambda_i\}_{i=1\dots n_R}, \{R_i\}_{i=1\dots n_R}) \\ & \quad \cdot \mathbb{P}(\{\lambda_i\}_{i=1\dots n_R} \mid \{x_i\}_{i=1\dots n}, \{R_i\}_{i=1\dots n_R}) \quad (14) \end{aligned}$$

Assuming a uniform prior $\lambda_i \sim \mathcal{U}(0, 1)$, we can rewrite the integrand as a product of two likelihoods:

$$\begin{aligned} & \mathbb{P}(\{y_i\}_{i=1\dots m} \mid \{\lambda_i\}_{i=1\dots n_R}, \{R_i\}_{i=1\dots n_R}) = \\ & \quad \mathbb{P}(\{x_i\}_{i=1\dots n} \mid \{R_i\}_{i=1\dots n_R})^{-1} \\ & \cdot \int d\lambda_1 d\lambda_2 \dots d\lambda_{n_R} \mathbb{P}(\{y_i\}_{i=1\dots m} \mid \{\lambda_i\}_{i=1\dots n_R}, \{R_i\}_{i=1\dots n_R}) \\ & \quad \cdot \mathbb{P}(\{x_i\}_{i=1\dots n} \mid \{\lambda_i\}_{i=1\dots n_R}, \{R_i\}_{i=1\dots n_R}) \quad (15) \end{aligned}$$

Given that we have a closed-form likelihood, it is possible to calculate the integrand numerically. This is still, however, an integral over variable λ with a dimensionality equal to the number of regions. One can numerically approximate this integral using Monte Carlo integration or methods such as nested sampling (Skilling, 2006; Buchner, 2023; Lemos et al., 2023a). We show an experiment using this Bayesian approach with a low number of regions in §B, but otherwise, given the numerical cost of this method, we will focus on the frequentist approach in this paper, and leave the Bayesian approach for future work.

3. Algorithmic Instantiation

Algorithm 1 The frequentist version of our algorithm

- 1: **Input:** Two sets of samples $\{x_i\}_{i=1\dots n} \sim p(x)$ and $\{y_i\}_{i=1\dots m} \sim q(y)$, a distance metric $d: X \times X \rightarrow \mathbb{R}$, a number of regions n_R
- 2: **Output:** A p-value
- 3: **Procedure:**
- 4: $x_{i=1\dots n_R}^{\text{ref}} \sim \{x_i\}_{i=1\dots n}$
- 5: $\text{counts}_x \leftarrow \{0\}_{i=1\dots n_R}$
- 6: $\text{counts}_y \leftarrow \{0\}_{i=1\dots n_R}$
- 7: **for** $i = 1$ **to** n **do**
- 8: $idx \leftarrow \text{argmin}_{j=1\dots n_R} d(x_i, x_j^{\text{ref}})$
- 9: $\text{counts}_x[idx] \leftarrow \text{counts}_x[idx] + 1$
- 10: **end for**
- 11: **for** $i = 1$ **to** m **do**
- 12: $idx \leftarrow \text{argmin}_{j=1\dots n_R} d(y_i, x_j^{\text{ref}})$
- 13: $\text{counts}_y[idx] \leftarrow \text{counts}_y[idx] + 1$
- 14: **end for**
- 15: $\chi_{\text{PQM}}^2 \leftarrow$ calculate from Eq. (11)
- 16: p-value \leftarrow calculate from Eq. (12)
- 17: **return** χ_{PQM}^2 , p-value

We now introduce an algorithmic instantiation of our framework. The key element in the algorithm is the choice of the regions $\{R_i\}_{i=1\dots n_R}$. We follow Lemos et al. (2023a) in us-

ing the *Tests of Accuracy with Random Points* (TARP) framework. We combine definition 7 and remark 2 of (Lemos et al., 2023a) in the following way:

Definition 3.1. Given a distance metric $d: U \times U \rightarrow \mathbb{R}$, every pair of points $(x_c, x_r) \sim U$ defines a TARP region as:

$$\{x \in U \mid d(\theta, x_c) \leq d(x_r, x_c)\} \quad (16)$$

In this case, however, we cannot randomly select regions from U . The reason for that is that the derivation of §2.2 assumes that the different regions do not overlap, which will not be the case if we randomly select regions from U . Therefore, we need to generate regions that do not overlap. We do this by noticing the following:

Lemma 3.2. A set of distinct points $\{x_i^{\text{ref}}\}_{i=1\dots n}$ defines a set of non-overlapping TARP regions, through the Voronoi tessellation of the space U .

$$R_i \equiv \{x \in U \mid d(x, x_i^{\text{ref}}) < d(x, x_j^{\text{ref}}) \forall i \neq j\} \quad (17)$$

i.e., the region R_i is defined by the points that are closest to the reference point that defines that region, x_i^{ref} , than to any other reference point.

The R_i partition the entire space into non-overlapping regions.¹ We show an illustration of the Voronoi tessellation in the right panel of Fig. 1, and the frequentist version of our algorithm in Algorithm 1.

4. Experiments

4.1. Null Test

We start by testing PQMass on a null test, where we know that the two sets of samples are equivalent. As our generative model, we use a Gaussian mixture model in 100 dimensions, with 20 components. We then repeat the following process 200 times: We generate 5000 samples from the Gaussian mixture model and then measure the χ_{PQM}^2 value of our test, with $n_R = 100$. We show the results in Fig. 2. We can see that the χ_{PQM}^2 value is distributed as a chi-squared distribution with $n_R - 1$ degrees of freedom, as expected from the discussion of §2.2.

This test, while simple, is important, as it shows that the proposed method is not biased towards rejecting the null hypothesis. More importantly, it shows our main result introduced in §2.2 in action. We show more such null tests for complex distributions in §A.

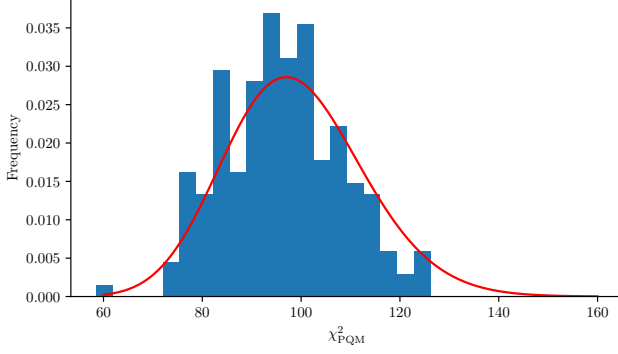


Figure 2. Null test. We generate two sets of samples from the same Gaussian mixture model in 100 dimensions. We then measure the χ^2_{PQM} value of our test ($n_R = 100$) and repeat this process 500 times, resampling every time. We can see that the χ^2_{PQM} value is distributed as a chi-squared distribution with $n_R - 1$ degrees of freedom, as expected.

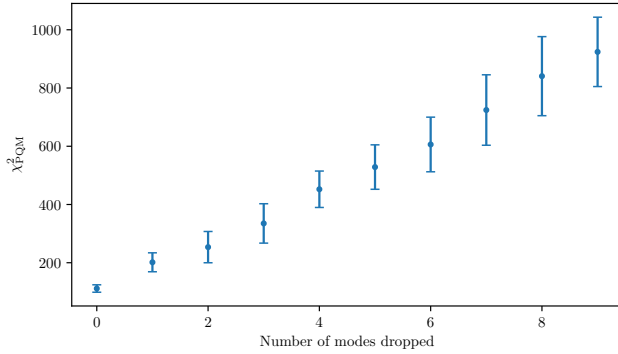


Figure 3. Gaussian Mixture Model. We show the results for PQMass on the Y axis, and the number of dropped modes on the X axis. We repeat the comparison 20 times, each time changing the reference points, and report the standard deviation. We can see that the χ^2_{PQM} value increases as we drop more modes, as expected.

4.2. Gaussian Mixture Model

For our second test, we re-use the Gaussian Mixture Model from §4.1. We use our test, dropping some of the modes from the Gaussian Mixture Model. For each number of modes, we first generate 5000 samples and then repeat our test 20 times with $n_R = 100$, changing the random reference points each time. We show the results in Fig. 3. We can see that the χ^2_{PQM} value increases as we drop more modes, as expected. This shows that PQMass can detect when a generative model is missing modes and, therefore, has poor

¹To be precise, there exists a set of points that are equidistant to two or more reference points. In this case, we could assign the point to the region of the reference point with the lowest index. However, this is an insignificant point, as the boundaries of the regions have measure zero if the points are drawn from a continuous distribution.

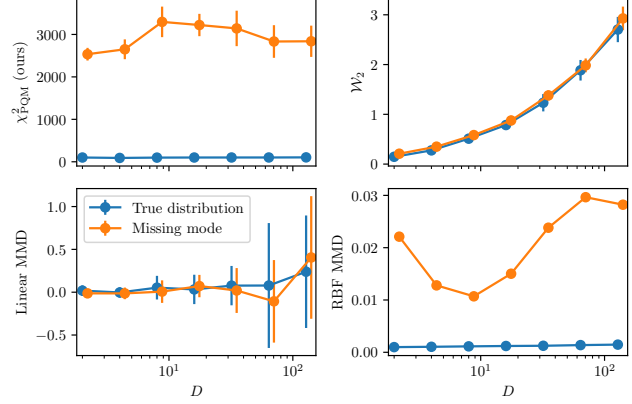


Figure 4. Differences in various sample-based metrics as a function of the dimensionality of the data. We use a mixture of 10 equally weighted Gaussians with varying numbers of dimensions. For each dimensionality, calculate the value of both metrics when comparing samples from the same distribution (blue) and from different distributions where one of them is missing one mode (orange), repeating the test various times to get an estimate of the noise. Ideally, we want our sample-based metrics to be able to detect that a mode has been dropped.

fidelity and diversity.

4.3. Validation of Sampling Methods

In this section, we show how we can use PQMass to study the performance of sampling algorithms as long as we have access to true samples from the probability distribution. Sampling methods are often evaluated on synthetic tasks, such as sampling from a Gaussian mixture model, for which we can generate true samples. Sample-based metrics that are commonly used to evaluate sampling methods include the Wasserstein distance, the Sinkhorn distance (Cuturi, 2013), the Kulback-Leibler divergence (Kullback & Leibler, 1951), the Jensen-Shannon divergence (Lin, 1991), among others. While these sample-based metrics work well on low-dimensional settings, they are not well suited for high-dimensional settings, as they require the calculation of integrals over the space of samples, or a density estimation step, which is not feasible in high dimensions.

On the other hand, the proposed method is only based on calculating distances between points and can, therefore, be easily applied to high-dimensional settings. Furthermore, the method does not make any assumptions about the underlying distribution and, therefore, can be applied to any distribution as long as we have access to true samples.

First, we compare PQMass to other sample-based metrics on a low-dimensional task, where we can use other traditionally used sample-based metrics. We use the two-dimensional Gaussian mixture model used in Midgley et al.

Table 1. Comparison of various sampling methods on a mixture model in $D = 2$ and a funnel in $D = 10$. We show the results for PQMass and compare them to the Wasserstein distance, the MMD with an RBF kernel, and the Jensen-Shannon divergence.

Model	Mixture Model ($D = 2$)				Funnel ($D = 10$)		
	$\chi^2_{\text{PQM}} (n_R = 100)$	\mathcal{W}_2	RBF MMD	JSD	$\chi^2_{\text{PQM}} (n_R = 100)$	\mathcal{W}_2	RBF MMD
MCMC	1621.06 ± 82.40	8.94	0.0151	0.42	855.40 ± 49.60	17.41	0.0566
FAB	678.22 ± 88.43	5.77	0.0038	0.39	96.69 ± 13.52	22.08	0.0032
GGNS	109.32 ± 12.36	3.2	0.0011	0.35	472.99 ± 18.00	32.20	0.0358

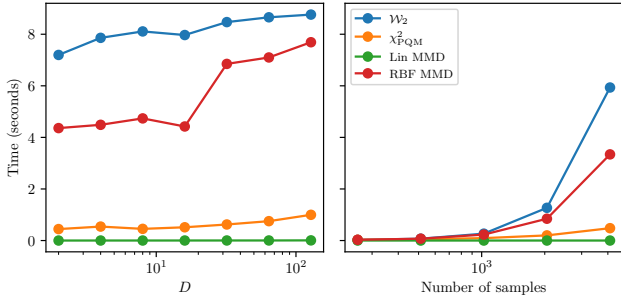


Figure 5. Computational cost of various sample-based metrics, as a function of the dimensionality of the data. For the same experiment as in Fig. 4, we show the time required to calculate the value of each metric, both as a function of the dimensionality of the data (left) and the number of samples (right).

(2022), which has been used for benchmarking various sampling methods. We generate samples using Flow annealed importance sampling bootstrap (FAB, Midgley et al., 2022) Markov Chain Monte Carlo (Metropolis et al., 1953), for which we use the `emcee` implementation (Foreman-Mackey et al., 2013), and Gradient-Guided Nested Sampling (GGNS, Skilling, 2006; Lemos et al., 2023b). For each method, we generate 10,000 samples and compare them with 10,000 samples from the true distribution. We calculate the Wasserstein distance, the Mean Maximum Discrepancy (MMD, Gretton et al., 2012) with a radial basis function (RBF) kernel and the Jensen-Shannon divergence (after performing a step of kernel density estimation); and compare them to the χ^2_{PQM} value of our test, with $n_R = 100$. For PQMass, we repeat this process 20 times, each time changing the reference points, and report the standard deviation. We show the results in Table 1. We can see that PQMass is in good agreement with the other sample-based metrics and that the χ^2_{PQM} value is correlated with the other sample-based metrics.

We then repeat this experiment on a higher dimensional task: Neal’s funnel distribution (Neal, 2003), a 10-dimensional distribution that is commonly used to benchmark sampling methods. We repeat the same experiment as before, except we do not use the Jensen-Shannon divergence, as it requires a density estimation step, which is not feasible in high di-

mensions. We see that PQMass is in good agreement with the MMD, while the Wasserstein distance follows a different pattern. We show samples from each model in §D, which show that, visually, PQMass captures the best-performing sampling methods.

There are, of course, multiple other methods for sampling, both deep learning based (such as Zhang & Chen, 2021; Lahlou et al., 2023; Richter et al., 2023, amongst many others) and non-deep learning based (e.g., Del Moral et al., 2006; Hoffman et al., 2014), that could have been added to Table 1. Furthermore, hyperparameter tuning could be used to improve the performance of each sampling method. The purpose of this table is not to compare different sampling methods but rather to show that PQMass can be used to evaluate sampling methods.

Finally, we study the scaling of PQMass with the dimensionality of the data. We use a mixture of 10 equally weighted Gaussians with varying numbers of dimensions. For each dimensionality, we generate 5,000 samples and compare them with 5,000 samples from the same distribution. We calculate the χ^2_{PQM} value of our test, with $n_R = 100$, as well as other sample-based metrics. We then repeat the experiment, dropping one mode and comparing the value of each metric. We do not compute the Kulback-Leibler or Jensen-Shannon divergence, as they require a density estimation step, which is not feasible in high dimensions. We show the results in Fig. 4. We can see that while \mathcal{W}_2 and linear MMD get increasingly noisier as the dimensionality increases, PQMass remains stable. MMD with an RBF kernel can also consistently highlight the difference between the two, however the computational cost of radial basis MMD scales far worse with dimensionality than PQMass. We show this in Fig. 5. We can see that the computational cost of PQMass scales much better with both dimensionality and number of samples than the Wasserstein and the MMD with an RBF kernel. MMD with a linear kernel is the cheapest computationally, but as shown in Fig. 4, it is too noisy to be usable in complex problems.

4.4. Time Series

For our next experiment, we show the flexibility of PQMass by applying it to a very different type of dataset: Time series

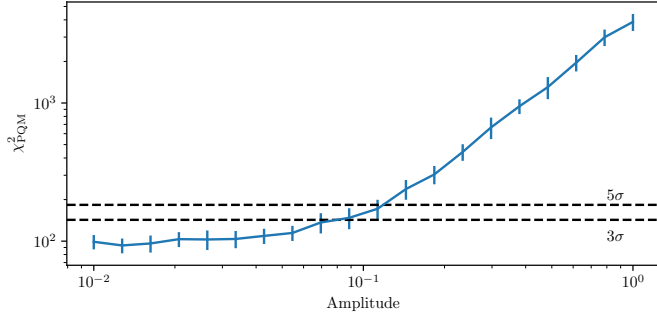


Figure 6. Time Series. We show the results for PQMass on the Y-axis and the amplitude of the signal on the X-axis. We repeat the comparison 5000 times, each time generating a time series with $A = 0$, and a time series with $A \neq 0$. We can see that the χ_{PQM}^2 value increases as A grows, as expected. We also show the values of χ_{PQM}^2 corresponding to the 3σ and 5σ significance levels of detection as black dashed lines.

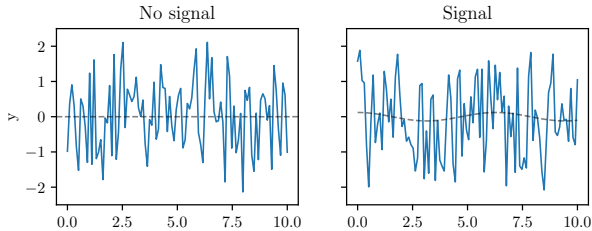


Figure 7. Examples of time series with $A = 0$ (left), and with $A \approx 0.12$ (right). PQMass can detect the signal with 5σ significance, a signal that is invisible to the naked eye (at least, to those of the authors).

data. We design the following experiment: We observe a noisy time series of fixed length, and we want to know if there is an underlying signal hiding in the noise. We generate the time series as follows: We generate the signal as:

$$y(t) = A \cdot \cos(t) + \eta(t), \quad (18)$$

where A is the amplitude of the signal and $\eta(t)$ is i.i.d. Gaussian noise with zero mean and unit variance. If $A = 0$, then the time series is just noise. If $A \neq 0$, then there is a signal hiding in the noise. For each observation, we generate 100 datapoints between $t = 0$ and $t = 10$. We then repeat the following process 5000 times: We generate a time series with $A = 0$ and a time series with $A \neq 0$. We then compare the two time series using PQMass, with $n_R = 100$. We show the results in Fig. 6 for varying values of A . We can see that the χ_{PQM}^2 value increases as A grows, as expected. The plot also the values of χ_{PQM}^2 corresponding to the 3σ and 5σ significance levels of detection. We see that, for this experiment, we can detect the signal with 5σ significance for $A \approx 0.12$, a signal that is invisible to the naked eye. We show an example of a time series with this amplitude,

compared to one without signal in Fig. 7.

This experiment serves to show the versatility of PQMass. Because we make no assumptions about the underlying distribution, we can apply PQMass to any type of data as long as we have access to samples. Detecting signals in noisy time series is a common problem in multiple disciplines, such as astronomy (Zackay et al., 2021; Aigrain & Foreman-Mackey, 2023), finance (Chan, 2004; Sezer et al., 2020), and anomaly detection (Ren et al., 2019; Shaukat et al., 2021). Existing methods rely on assumptions about the underlying distribution. PQMass, on the other hand, can detect that the observed signal is not consistent with samples of random noise with no assumptions on the generative process. We leave the application of PQMass to these domains for future work.

4.5. Training a Generative Model

In this section, we track the value of our metric as we train two generative models, a variational autoencoder (VAE; Kingma & Welling, 2013) and a denoising diffusion model (Ho et al., 2020a; Song et al., 2021) with hyperparameters detailed in §E. We train on the MNIST² dataset and compare generated samples with the MNIST test set. After each epoch of training is completed, we generate 2000 samples and compute χ_{PQM}^2 with $n_R = 100$. We execute this experiment over the first 100 epochs to highlight the early stages of training for the models and repeat the experiment twice for robustness. We see in Fig. 8 that as training continues, the metric begins to stabilize with fluctuations due to the unique samples generated at each epoch. For the VAEs, we see that the samples can capture high-level structures, but they struggle to capture the complex features. Whereas the diffusion models, the generated samples are similar to the true distribution as seen by their low χ_{PQM}^2 values, which plateau at around $\chi_{PQM}^2 \sim 99$ as expected.

The use of the metric for the generative model gives the ability to track the quality of the model’s performance relative to the true distribution, preserving the integrity of the underlying data structure and without any loss of dimensionality. Therefore, given samples from the true distribution (i.e. a test set), this approach can be used as a method to indicate performance throughout the training of a generative model.

4.6. Image Datasets

In this section, we test PQMass on image datasets. We use samples from Stein et al. (2023), which contains samples from various image datasets, and various generative models. We focus on the CIFAR-10 dataset³. Following (Stein et al., 2023), we first use the human error rate as a measure of the

²<http://yann.lecun.com/exdb/mnist/>

³<https://www.cs.toronto.edu/~kriz/cifar.html>

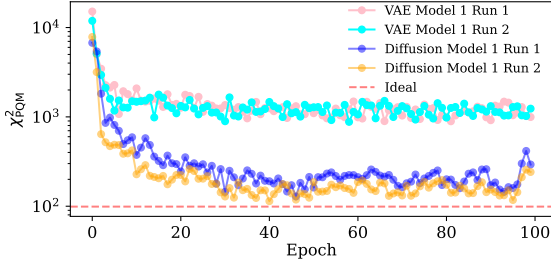


Figure 8. After each training epoch for the different models is completed, we generate samples and compute the χ^2 metric to assess the quality against the true distribution. We perform this experiment twice, Run 1 and Run 2 for each model respectively, and see χ^2_{PQM} values agree with each other even as they generate unique samples each time. The diffusion model can achieve χ^2_{PQM} near ideal (χ^2_{PQM} equal to the number of degrees of freedom $n_R - 1$, in this case 99), indicating its ability to learn the underlying distribution.

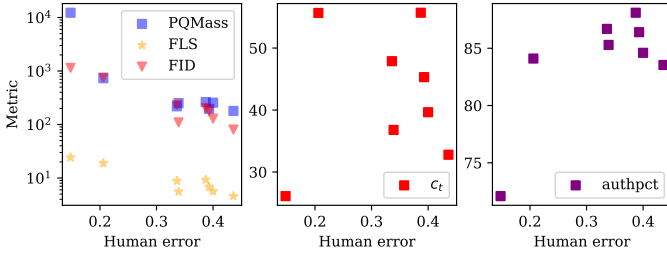


Figure 9. Correlation of human error rate in identifying real images with various sample-based metrics (results of prior methods taken from Jiralerspong et al. (2023)). The result for PQMass is the χ^2_{PQM} value averaged over 20 samples. PQMass estimates the fidelity and diversity of generative models well despite not relying on a feature representation, unlike FLS and FID.

fidelity and diversity of the generative models. We compare generated samples from each of the models, to the test data for CIFAR-10. We repeat the comparison 20 times, each time varying the reference points. We show the results for CIFAR-10 in Fig. 9. We find that our chi-squared values strongly correlate with the human error rate, indicating that PQMass can measure the fidelity and diversity of generative models.

One key strength of PQMass is its scaling to high-dimensional problems. Unlike alternative methods such as FID and FLS, PQMass does not require using a feature extractor to reduce the dimensionality of the problem. Therefore, we can use PQMass to compare generative models on high-dimensional problems and do not risk potential biases introduced by the feature extractor.

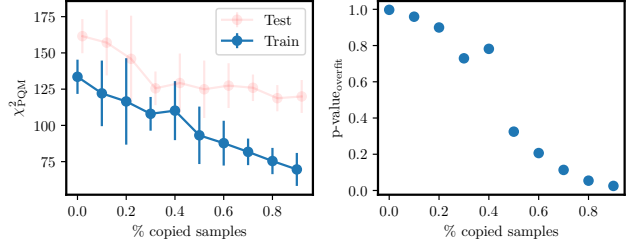


Figure 10. Novelty. PQMass (Y axis) when a fraction of the generated samples are replaced by samples taken from the training set (X axis). We repeat the comparison 20 times, each time changing the reference points, and report the standard deviation. We show the value of χ^2_{PQM} in the left panel, for the test (red) and train (blue), and the p-value for the training data on the left. We see that, as memorization increases, the gap between the train and test χ^2_{PQM} increases and the p-value goes down.

4.7. Novelty

One important aspect of generative models is their novelty: We want to know if the generative model generates samples that are novel or if it simply copies the training data. While PQMass can measure the fidelity and diversity of generative models, it cannot directly measure their novelty. There are two approaches we can follow to detect memorization: The first one is to follow Jiralerspong et al. (2023), in looking at the *generalization gap* for PQMass, i.e., how our metric changes when comparing the generated samples to the training data and when comparing the generated samples to the validation data. The second one is to look at the value of χ^2_{PQM} on the training data directly. Indeed, we know that a value that is too low is indicative of overfitting. For a large number of regions (i.e., degrees of freedom), we know the chi-square distribution is approximately Gaussian. Therefore, we can use the symmetry of this distribution (as shown in Fig. 2, to get a p-value that penalizes suspiciously low values of χ^2_{PQM} by considering the mirror reflection of the chi-square value around the maximum:

$$\text{p-value}_{\text{overfit}}(\chi^2_{PQM}) \equiv \int_{-\infty}^{2n_R - \chi^2_{PQM}} \chi^2_{n_R - 1}(z) dz. \quad (19)$$

To study this, we repeat the ‘copycat’ experiment of (Jiralerspong et al., 2023): We pick one of the models used in §4.6, and repeat our test, replacing some fraction of the generated samples with samples from the training data. We then calculate the χ^2_{PQM} value of our test, first comparing the generated samples to the training data and then comparing the generated samples to the validation data.

We show the results for PFGMPP in Fig. 10. The left panel shows that the gap between χ^2_{PQM} when compared to the training data and χ^2_{PQM} value when comparing to the validation data is larger the more samples we replace. The right

panel shows the two-sided p-value, which clearly goes down as the number of copied samples increases. This shows that both of these methods (generalization gap and two-sided p-value) can be used to detect memorization in generative models.

5. Conclusions

In this paper, we have introduced a new method for quantifying the probability that two sets of samples are drawn from the same probability distribution. PQMass is based on comparing the probability mass of the two sets of samples in a set of non-overlapping regions. It relies only on the calculation of distances between points and, therefore, can be applied to high-dimensional problems. It does not require training or fitting any models. Furthermore, it does not require any assumptions about the underlying distribution and, therefore, can be applied to any type of data as long as we have access to true samples. We have shown that PQMass can be used to evaluate sampling methods and track the performance of generative models as they train.

We have shown the performance of PQMass on a variety of synthetic tasks, as well as on comparing sampling methods, comparing generative models of images, and detecting hidden signals in time series. Given the versatility and low computational cost of PQMass, it can serve as a valuable tool for evaluating the quality and performance of generative models and sampling methods.

Acknowledgments

This research was made possible by a generous donation by Eric and Wendy Schmidt with the recommendation of the Schmidt Futures Foundation. This work is also supported by the Simons Collaboration on "Learning the Universe". The work is in part supported by computational resources provided by Calcul Quebec and the Digital Research Alliance of Canada. Y.H. and L.P. acknowledge support from the Canada Research Chairs Program, the National Sciences and Engineering Council of Canada through grants RGPIN-2020-05073 and 05102, and the Fonds de recherche du Québec through grants 2022-NC-301305 and 300397. N.M. acknowledges funding from CIFAR, Genentech, Samsung, and IBM.

We thank Adam Coogan, Sebastian Wagner-Carena, Joey Bose, Gauthier Gidel, Alex Tong, Alexandra Volokhova and Marco Jiralespong for very inspiring discussions, and feedback on early versions of this work. We also thank Marco Jiralespong for sharing useful data.

Reproducibility Statement

An implementation of PQMass, along with notebooks to reproduce the results from the experiments will be released upon publication.

Impact Statement

As a robust and efficient algorithm for measuring discrepancies between sets of samples in high dimensions, PQMass can be used in the assessment of ML models as well as in scientific or industrial applications. The ability of PQMass to distinguish machine-generated and naturally occurring data distributions has implications for the detection of synthetic content, which is especially important in light of the growing emphasis on the interaction of AI systems with intellectual property, human rights, and social welfare.

References

- Aigrain, S. and Foreman-Mackey, D. Gaussian process regression for astronomical time series. *Annual Review of Astronomy and Astrophysics*, 61:329–371, 2023.
- Alaa, A., Breugel, B., Saveliev, E., and Schaar, M. How faithful is your synthetic data. *Sample-Level Metrics for Evaluating and Auditing Generative Models*. *arXiv*, 2022.
- Anderson, D. A., McDonald, L. L., and Weaver, K. D. Tests on categorical data from the unionintersection principle. *Annals of the Institute of Statistical Mathematics*, 26:203–213, 1974.
- Bastian, P., Dette, H., and Koletzko, L. Testing equivalence of multinomial distributions—a constrained bootstrap approach. *Statistics & Probability Letters*, 206:109999, 2024.
- Buchner, J. Nested sampling methods. *Statistic Surveys*, 17:169–215, 2023.
- Chan, N. H. *Time series: applications to finance*. John Wiley & Sons, 2004.
- Cuturi, M. Sinkhorn distances: Lightspeed computation of optimal transport. *Advances in neural information processing systems*, 26, 2013.
- Del Moral, P., Doucet, A., and Jasra, A. Sequential monte carlo samplers. *Journal of the Royal Statistical Society Series B: Statistical Methodology*, 68(3):411–436, 2006.
- Foreman-Mackey, D., Hogg, D. W., Lang, D., and Goodman, J. emcee: the mcmc hammer. *Publications of the Astronomical Society of the Pacific*, 125(925):306, 2013.
- Goodfellow, I., Pouget-Abadie, J., Mirza, M., Xu, B., Warde-Farley, D., Ozair, S., Courville, A., and Bengio, Y.

- Generative adversarial nets. *Advances in neural information processing systems*, 27, 2014.
- Gretton, A., Borgwardt, K. M., Rasch, M. J., Schölkopf, B., and Smola, A. A kernel two-sample test. *The Journal of Machine Learning Research*, 13(1):723–773, 2012.
- Heusel, M., Ramsauer, H., Unterthiner, T., Nessler, B., and Hochreiter, S. Gans trained by a two time-scale update rule converge to a local nash equilibrium. *Advances in neural information processing systems*, 30, 2017.
- Ho, J., Jain, A., and Abbeel, P. Denoising diffusion probabilistic models. In Larochelle, H., Ranzato, M., Hadsell, R., Balcan, M., and Lin, H. (eds.), *Advances in Neural Information Processing Systems*, volume 33, pp. 6840–6851. Curran Associates, Inc., 2020a. URL <https://proceedings.neurips.cc/paper/2020/file/4c5bcfec8584af0d967f1ab10179ca4b-Paper.pdf>.
- Ho, J., Jain, A., and Abbeel, P. Denoising diffusion probabilistic models. *Advances in neural information processing systems*, 33:6840–6851, 2020b.
- Hoffman, M. D., Gelman, A., et al. The no-u-turn sampler: adaptively setting path lengths in hamiltonian monte carlo. *J. Mach. Learn. Res.*, 15(1):1593–1623, 2014.
- Jiralerspong, M., Bose, A. J., and Gidel, G. Feature likelihood score: Evaluating generalization of generative models using samples. *arXiv preprint arXiv:2302.04440*, 2023.
- Kingma, D. P. and Welling, M. Auto-Encoding Variational Bayes. *arXiv e-prints*, art. arXiv:1312.6114, December 2013. doi: 10.48550/arXiv.1312.6114.
- Kingma, D. P. and Welling, M. Auto-encoding variational bayes. *arXiv preprint arXiv:1312.6114*, 2013.
- Kullback, S. and Leibler, R. A. On information and sufficiency. *The annals of mathematical statistics*, 22(1): 79–86, 1951.
- Lahlou, S., Deleu, T., Lemos, P., Zhang, D., Volokhova, A., Hernández-García, A., Ezzine, L. N., Bengio, Y., and Malkin, N. A theory of continuous generative flow networks. In *International Conference on Machine Learning*, pp. 18269–18300. PMLR, 2023.
- Le Lan, C. and Dinh, L. Perfect density models cannot guarantee anomaly detection. *Entropy*, 23(12):1690, 2021.
- Lemos, P., Coogan, A., Hezaveh, Y., and Perreault-Levasseur, L. Sampling-based accuracy testing of posterior estimators for general inference. *arXiv preprint arXiv:2302.03026*, 2023a.
- Lemos, P., Malkin, N., Handley, W., Bengio, Y., Hezaveh, Y., and Perreault-Levasseur, L. Improving gradient-guided nested sampling for posterior inference. *arXiv preprint arXiv:2312.03911*, 2023b.
- Lin, J. Divergence measures based on the shannon entropy. *IEEE Transactions on Information theory*, 37(1):145–151, 1991.
- Metropolis, N., Rosenbluth, A. W., Rosenbluth, M. N., Teller, A. H., and Teller, E. Equation of state calculations by fast computing machines. *The journal of chemical physics*, 21(6):1087–1092, 1953.
- Midgley, L. I., Stimper, V., Simm, G. N., Schölkopf, B., and Hernández-Lobato, J. M. Flow annealed importance sampling bootstrap. *arXiv preprint arXiv:2208.01893*, 2022.
- Nalisnick, E., Matsukawa, A., Teh, Y. W., Gorur, D., and Lakshminarayanan, B. Do deep generative models know what they don’t know? *arXiv preprint arXiv:1810.09136*, 2018.
- Neal, R. M. Slice sampling. *The annals of statistics*, 31(3): 705–767, 2003.
- Nowozin, S., Cseke, B., Tomioka, R., and GAN. Training generative neural samplers using variational divergence minimization. In *Proc. Adv. Neural Inf. Process. Syst.*, pp. 271–279.
- Plunkett, A. and Park, J. Two-sample test for sparse high-dimensional multinomial distributions. *Test*, 28:804–826, 2019.
- Rao, C. Karl pearson chi-square test the dawn of statistical inference. *Goodness-of-fit tests and model validity*, pp. 9–24, 2002.
- Rao, C. R. Tests of significance in multivariate analysis. *Biometrika*, 35(1/2):58–79, 1948.
- Ren, H., Xu, B., Wang, Y., Yi, C., Huang, C., Kou, X., Xing, T., Yang, M., Tong, J., and Zhang, Q. Time-series anomaly detection service at microsoft. In *Proceedings of the 25th ACM SIGKDD international conference on knowledge discovery & data mining*, pp. 3009–3017, 2019.
- Rezende, D. and Mohamed, S. Variational inference with normalizing flows. In *International conference on machine learning*, pp. 1530–1538. PMLR, 2015.
- Richter, L., Berner, J., and Liu, G.-H. Improved sampling via learned diffusions. *arXiv preprint arXiv:2307.01198*, 2023.

- Sajjadi, M. S., Bachem, O., Lucic, M., Bousquet, O., and Gelly, S. Assessing generative models via precision and recall. *Advances in neural information processing systems*, 31, 2018.
- Salimans, T., Goodfellow, I., Zaremba, W., Cheung, V., Radford, A., and Chen, X. Improved techniques for training gans. *Advances in neural information processing systems*, 29, 2016.
- Salimans, T., Zhang, H., Radford, A., and Metaxas, D. Improving gans using optimal transport. *arXiv preprint arXiv:1803.05573*, 2018.
- Sezer, O. B., Gudelek, M. U., and Ozbayoglu, A. M. Financial time series forecasting with deep learning: A systematic literature review: 2005–2019. *Applied soft computing*, 90:106181, 2020.
- Shaukat, K., Alam, T. M., Luo, S., Shabbir, S., Hameed, I. A., Li, J., Abbas, S. K., and Javed, U. A review of time-series anomaly detection techniques: A step to future perspectives. In *Advances in Information and Communication: Proceedings of the 2021 Future of Information and Communication Conference (FICC), Volume 1*, pp. 865–877. Springer, 2021.
- Skilling, J. Nested sampling for general bayesian computation. 2006.
- Song, Y., Sohl-Dickstein, J., Kingma, D. P., Kumar, A., Ermon, S., and Poole, B. Score-based generative modeling through stochastic differential equations. In *International Conference on Learning Representations*, 2021. URL <https://openreview.net/forum?id=PxtTIG12RRHS>.
- Stein, G., Cresswell, J. C., Hosseinzadeh, R., Sui, Y., Ross, B. L., Vिलецрозе, V., Liu, Z., Caterini, A. L., Taylor, J. E. T., and Loaiza-Ganem, G. Exposing flaws of generative model evaluation metrics and their unfair treatment of diffusion models. *arXiv preprint arXiv:2306.04675*, 2023.
- Szegedy, C., Vanhoucke, V., Ioffe, S., Shlens, J., and Wojna, Z. Rethinking the inception architecture for computer vision. In *Proceedings of the IEEE conference on computer vision and pattern recognition*, pp. 2818–2826, 2016.
- Theis, L., Oord, A. v. d., and Bethge, M. A note on the evaluation of generative models. *arXiv preprint arXiv:1511.01844*, 2015.
- Yazici, Y., Foo, C.-S., Winkler, S., Yap, K.-H., and Chandrasekhar, V. Empirical analysis of overfitting and mode drop in gan training. In *2020 IEEE International Conference on Image Processing (ICIP)*, pp. 1651–1655. IEEE, 2020.
- Zackay, B., Venumadhav, T., Roulet, J., Dai, L., and Zaldarriaga, M. Detecting gravitational waves in data with non-stationary and non-gaussian noise. *Physical Review D*, 104(6):063034, 2021.
- Zelterman, D. Goodness-of-fit tests for large sparse multinomial distributions. *Journal of the American Statistical Association*, 82(398):624–629, 1987.
- Zhang, Q. and Chen, Y. Path integral sampler: a stochastic control approach for sampling. *arXiv preprint arXiv:2111.15141*, 2021.

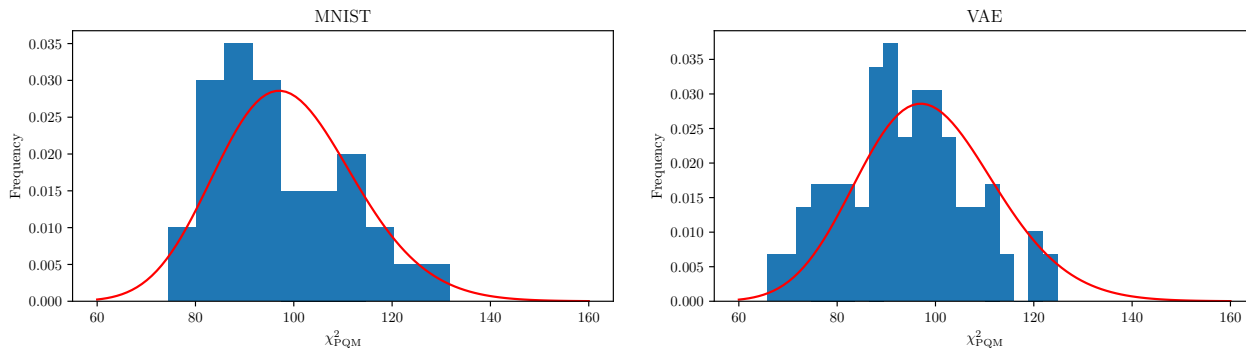


Figure 11. Null tests, similar to the one shown in Fig. 2, but for two different distributions: Samples from MNIST (left) and a VAE trained on MNIST (right). The main result of our paper holds for samples from any distribution as long as we are comparing two sets of independent samples from the same distribution. Note that, on MNIST, the fit is not perfect due to the limited number of data points.

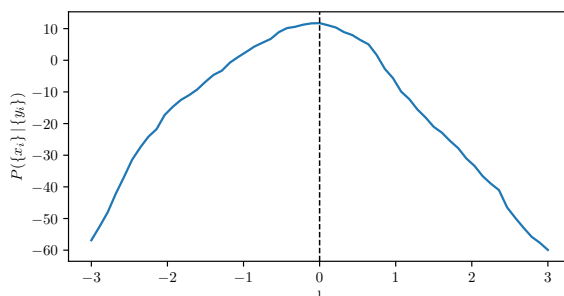


Figure 12. Log-probability of various models (translationally shifted by l) given a test dataset from a ground truth distribution. This probability is calculated using the Bayesian method described in Eq. 15. The ground truth distribution corresponds to $l = 0$.

A. Null Tests

The main result of this paper, shown in §2.2, was shown in practice in §4.1 for a high-dimensional mixture of Gaussians. In this section, we show that it works in even more complex and high-dimensional distributions. First, we test it on the MNIST data: Using the MNIST observations themselves as samples from some underlying probability distribution. We put together the MNIST train and test data, leading to 70,000 images. We then split them into two subsets of 35,000 images each. To repeat the null test of §4.1, we need independent samples at every iteration (note that this is different from the error bars reported in the rest of the experiments, which just arise from repeating with random tessellations, but always the same samples). Therefore, for each iteration, we take 1,000 images from each dataset, and perform the PQM test with $n_R = 100$, leading to 35 data points. We plot their histogram in the left panel of Fig. 11. While noisy, due to the very few data points, we see that the histogram does follow a chi-squared distribution with $n_R - 1$ degrees of freedom, as expected.

For our second experiment, we use one of the MNIST generative models described in §4.5. In this case, we can generate as many samples as we want. Because we are comparing the generative model to itself, the similarity of the generated samples to the MNIST train or test data is irrelevant for this particular test.

B. Bayesian Experiment

In this experiment, we numerically test the validity of the Bayesian method described in Eq. 15. This involved integrating the product of two multinomial distributions to determine the probability of a model given the training data. The setup mirrors that of the previous Gaussian Mixture Model experiment: we created a ‘ground-truth’ distribution, a Gaussian Mixture Model in 100 dimensions with 20 components. The means and variances of these components were randomly selected. From this mixture, we drew 5000 samples to form the test set.

Model	Default	$n_R = 50$	$n_R = 200$	L1 Distance	Inception
ACGAN-Mod	12407 ± 10	10410 ± 808	14125 ± 995	12336 ± 944	7891 ± 1009
LOGAN	713 ± 72	408 ± 69	1180 ± 95	728 ± 108	5750 ± 535
BigGAN-Deep	268 ± 30	135 ± 16	498 ± 36	238 ± 32	615 ± 74
iDDPM-DDIM	238 ± 22	143 ± 17	470 ± 41	244 ± 31	533 ± 78
MHGAN	234 ± 39	123 ± 19	470 ± 48	194 ± 18	628 ± 64
StyleGAN-XL	230 ± 13	119 ± 15	477 ± 23	203 ± 23	199 ± 19
StyleGAN2-ada	207 ± 26	128 ± 25	417 ± 48	197 ± 23	259 ± 30
PFGMPP	177 ± 22	108 ± 18	335 ± 28	175 ± 16	239 ± 28

Table 2. Ablation study for CIFAR-10. We repeat the experiment of §4.6, varying the number of reference points, as well as changing the distance metric to L1. We show the results for the frequentist version of PQMass, sorted in order of decreasing χ^2_{PQM} for the default version. We find that the results are robust to the choice of the number of reference points and the distance metric. Any observed differences are within the standard deviation of the experiment.

We then introduced a shift to this distribution along the diagonal direction (characterized by a vector of ones in 100 dimensions) multiplied by a scalar magnitude l . The resulting models, parameterized by l , were considered as potential generative models, aligning with the ground truth when $l = 0$. Note that this is an arbitrary choice to construct a family of competing models.

Three non-overlapping regions were then defined by selecting three random points and constructing a Voronoi tessellation. We formed a regularly spaced grid over the values of λ_1 and λ_2 (representing the probability mass in the first two regions), ensuring that λ_3 was chosen to allow the combination of the three values to be appropriately normalized.

We drew samples for each model (defined by different l values on a regularly spaced grid) and calculated the model’s probability with Eq. (15). This was achieved by computing the appropriately normalized multinomial distributions for the test data and the model data within the three regions and then integrating their product. This integration was done by summing across all grid points in the probability mass and multiplying by the volume of each grid point’s probability.

Fig. 12 shows the results: the left panel illustrates the log probability, while the right panel presents the (un-normalized) probability of the models as a function of the single parameter l . As anticipated, the correct model ($l = 0$) has a high probability, with the probability dropping as l diverges from this value. Employing a greater number of smaller regions could enhance the constraining power; however, this would require a sample-based integration method over the unknown λ values.

C. Ablation Study

In this section, we study the effect of varying the two hyperparameters of our experiment: The number of reference points n_R , and the distance metric (which in all experiments in the main text is L2). We repeat the experiment on CIFAR10 described in §4.6, varying the number of reference points, as well as changing the distance metric to L1. We also show the results when using the Inception-v3 feature extractor (Szegedy et al., 2016), as done in previous work such as (Jiralerspong et al., 2023). We find that the order of the models is robust to the choice of the number of reference points and the distance metric, as well as to the use of a feature extractor. Any observed differences are within the standard deviation of the experiment. We show the results in Table 2.

D. Samples for Validation

In §4.3, we showed the performance of PQMass, comparing samples from various sampling algorithms to true distribution samples. Fig. 13 shows the samples from each algorithm and the underlying distribution. For the Gaussian Mixture Model (top), we see that MCMC is missing a mode, while in FAB the samples are too noisy; for Neal’s funnel (bottom), we see that FAB’s samples look indistinguishable from true samples, while GGNS look similar but more spread out, and GFN and MCMC fail to model this distribution. In both cases, the results from χ^2_{PQM} correlate well with the similarity to true samples we can see by eye.

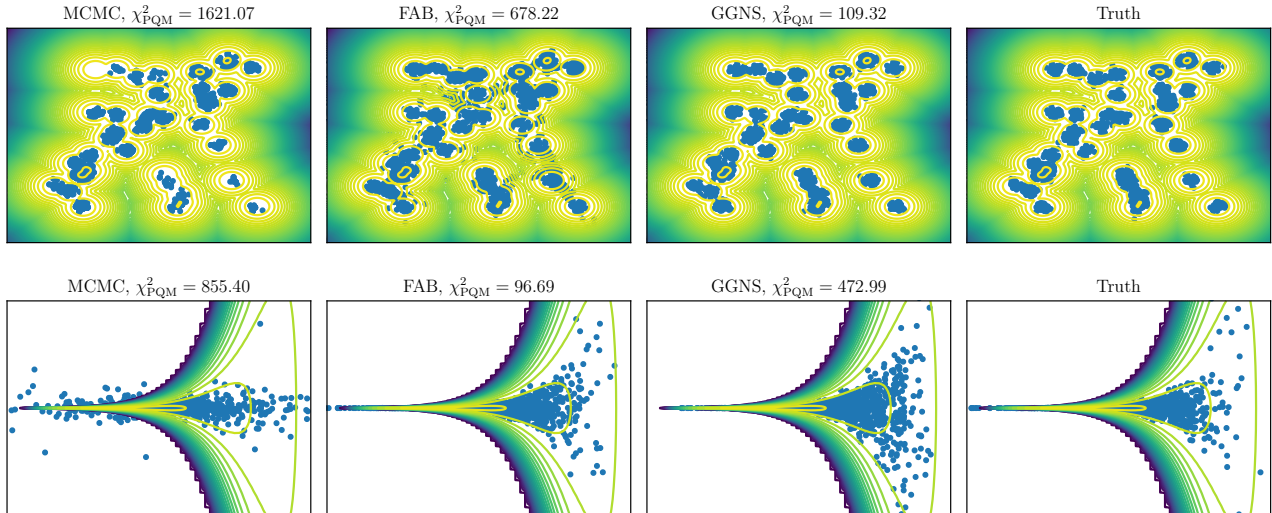


Figure 13. Samples from our the various sampling methods introduced in §4.3, and their corresponding PQMass values.

E. Generative Model Hyperparameters

In this section, we detail the hyper-parameters used for the respective models in §4.5. We first note that we use the MNIST data with the channel set to 1, since it is grayscale, and the spatial dimensions are 28×28 . For the variational autoencoder (VAE), the batch size is defined to be 512. For the encoder, the first layer maps from 784 dimensions to 512, followed by a second layer, reducing it further to 256 dimensions. The latent space was represented with 20 dimensions, as determined by the output of the subsequent layers. The Decoder architecture was the same, progressively reconstructing the data from the 20-dimensional latent space back to the original 784-dimensional space. We utilize the Adam optimizer with the learning rate initially set to 0.001. We also include a scheduler to reduce the learning rate every 50 steps by 0.1. For the denoising diffusion model, we use the package `score_models`⁴. Our model utilizes the NCSN++ architecture with Variance Preserving Stochastic Differential Equation (SDE). The batch size is defined to be 256 with a learning rate of 0.001 and exponential moving average decay of 0.999.

⁴https://github.com/AlexandreAdam/torch_score_models